

A Nanomechanical Mass Sensor with Yoctogram Resolution

Supplementary Information

J. Chaste¹, A. Eichler¹, J. Moser¹, G. Ceballos¹, R. Rurali², A. Bachtold¹

¹ Catalan Institute of Nanotechnology, CIN2 (ICN-CSIC), Campus de la UAB, 08193 Bellaterra (Barcelona), Spain

² Institut de Ciència de Materials de Barcelona (ICMAB-CSIC), Campus de la UAB, 08193 Bellaterra (Barcelona), Spain

A- Experimental setup

The measurement setup consists of an ultra-high vacuum (UHV) chamber where the device can be cooled down to 4 K (Fig. S1). A vacuum of $\sim 3 \cdot 10^{-11}$ mbar is reached after baking the setup at 125 C during ~ 2 days. The device is attached to the cold finger of a liquid helium insert (ST-400 from Janis) whose temperature can be varied between 4 and 400 K. The device is electrically connected with radio-frequency cables that are UHV compatible (Allectra 380-SMA-MF-500). The chamber is also equipped with a moveable stage (to move the helium insert with respect to the chamber), pressure gauges, and a mass spectrometer.

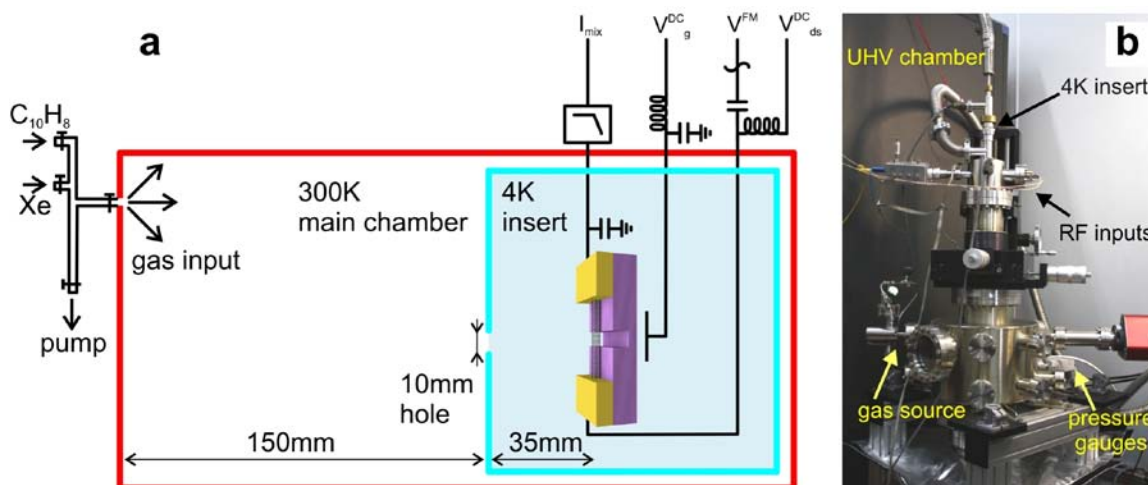


Fig. S1 a,b. Schematic and photograph of the UHV chamber.

The chamber is equipped with a pinhole microdoser in order to admit Xe atoms or naphthalene molecules into the vacuum chamber. Xe atoms are introduced into the

chamber from a gas reservoir at 300 K. As for naphthalene molecules, unwanted contaminants are removed by freeze-pump cycles of the gas reservoir prior to adsorption experiments.

The rate of Xe atoms or naphthalene molecules that impinge on the nanotube is set by the pressure in the main chamber. The atomic flux at the level of the 10 mm diameter hole in Fig. 1Sa is given by $P / \sqrt{2\pi mk_b T}$ with P the pressure in the main chamber, m the mass of a Xe atom or a naphthalene molecule, k_b the Boltzmann constant and T the temperature in the main chamber (300K). The atomic flux at the level of the nanotube is approximated by $S / 2\pi h^2 \cdot P / \sqrt{2\pi mk_b T}$ with S the surface of the 10 mm diameter hole and $h = 35$ mm the hole-nanotube distance.

The measurements shown in Fig. 3b were carried out at a naphthalene dosing pressure of $P = 1 \cdot 10^{-7}$ mbar. Since the diameter of the nanotube is 1.7 nm and its length is 150 nm, we calculate that one naphthalene molecule impinges on the nanotube on average every ~ 3 s.

When we are not dosing, the pressure can be as low as $\sim 3 \cdot 10^{-11}$ mbar. Assuming that the rest gas consists mainly of water molecules, we calculate that the expected time between two impinging events is about 3200 s.

The measurements in Fig. 3a are carried out with the moveable stage positioned so that Xe atoms arrive directly from the microdoser onto the nanotube. In this setup configuration, the chamber pressure does not allow us to estimate the dosing rate.

The motion of the nanotube is driven and detected using the frequency modulation (FM) mixing technique [1,2] (Fig. S1a). We apply a frequency modulated excitation V^{FM} on the source electrode using a 20 dB attenuator, a bias-tee, and coaxial cables that are UHV compatible. The resulting mixing current I_{mix} (at typically 671 Hz) is detected at the drain electrode using a lock-in amplifier, a 1nF capacitance to the ground at 4K, cryocoax cables, and a 1MHz filter at 300K. The I_{mix} response as a function of the driving frequency is shown schematically in Fig. S2.

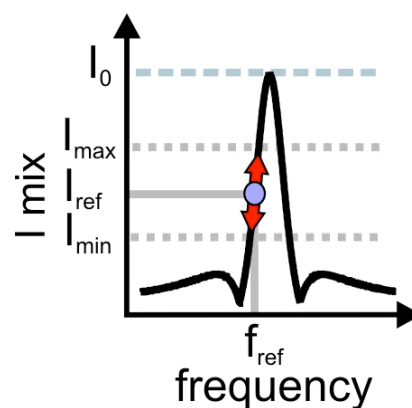


Fig. S2 Schematic of the response of the mixing current as a function of driving frequency.

The computer-controlled feedback loop aims at keeping I_{mix} around a reference value (I_{ref}) by varying f . When I_{mix} remains between I_{min} and I_{max} in Fig. S2, the driving frequency is not changed and, accordingly, the shift of the resonance frequency is calculated from I_{mix} and the slope of the resonance around I_{ref} . The feedback time can be made as low as 15 ms. The feedback is interrupted repeatedly (typically every 150 s) during ~5 s for a control of the lineshape of the resonance (I_{mix} as a function of f): if the resonance lineshape significantly differs from that measured previously, the recorded data are discarded. When f_0 shifts by a large amount due to e.g. the adsorption of a molecule, I_{mix} goes usually to 0 and, accordingly, the computer scans f over ~5 MHz to retrieve the resonance.

Here, we indicate typical parameters used in the computer-controlled feedback loop. We often set the reference current to $0.5 I_0$ on the low frequency part of the resonance, I_0 being the highest current of the resonance; but I_{ref} can also be lowered down to $0.3 I_0$ where the slope of the resonance is steeper. We set the thresholds I_{max} and I_{min} so that $(I_{max} - I_{min}) / I_0$ is typically 0.5 (we also tried values between 0.1 and 0.7). The current range $(I_{max} - I_{min})$ corresponds to a frequency range that is typically about 400 kHz. The computer-controlled feedback loop converts f_{ref} to f_0 using the stored resonance curve.

B- Mechanical resonator: effective mass and mass responsivity

Nanotube resonators can be described as harmonic oscillators with an effective mass m_{eff} , a spring constant k , and a mechanical resonance frequency $f_0 = 1/2\pi \cdot \sqrt{k/m_{eff}}$.

The effective mass depends on the mass of the nanotube m_{NT} as

$$m_{eff} = m_{NT} \frac{1}{L} \int_0^L [\varphi(x)]^2 dx \quad (S1)$$

with L the nanotube length and $\varphi(x)$ the shape of the eigenmode normalized so that $\max[\varphi(x)] = 1$.

When a mass δm is added to the resonator at position x_0 , the resonance frequency decreases as

$$\delta f_0 = -\frac{\delta m}{2m_{eff}} f_0 [\varphi(x_0)]^2 \quad (S2)$$

The shift of f_0 is 0 when δm is added nearby the clamping electrode ($\varphi(x_0) = 0$) whereas it is $-\delta m / 2m_{eff} \cdot f_0$ when δm is added at the position $\varphi(x_0) = 1$ (which is the

middle of the resonator in the case of the fundamental eigenmode). See the supplementary information of Ref. 3 for the derivation of eq. S2.

Assuming that the mass δm impinges on the tube at random locations, we obtain that the frequency shift is on average

$$\langle \delta f_0 \rangle = -\frac{\delta m}{2m_{NT}} f_0 \quad (\text{S3})$$

The nanotube in Fig. 1-3 has a length L_{NT} of ~150 nm and a diameter d of 1.7 nm.

We calculate that the mass of the nanotube is $m_{NT} = 6 \cdot 10^{-19}$ g using

$m_{NT} = 2m_C \cdot (\pi d L_{NT}) / A$ with m_C the mass of a carbon atom and $A = 5.2 \cdot 10^{-20}$ m² the surface of the hexagon in the honeycomb lattice of graphene. The effective mass is $m_{eff} = 3 \cdot 10^{-19}$ g since the nanotube is under tension (which is induced by applying a voltage to the gate electrode) and that the shape of the eigenmode can be approximated by $\varphi(x) = \sin(\pi x / L_{NT})$.

We estimate from our AFM images that the uncertainty in the measured diameter is ± 0.3 nm and that in the measured length is ± 15 nm. As a result, we get that $m_{eff} = 3 (\pm 0.8) \cdot 10^{-19}$ g. It would be useful in future mass sensing experiments to find a calibration method that does not rely on the precise mass of the nanotube. One possibility is to engineer single trapping sites in order to have a direct measure of the mass, which is not affected by the random location of the atoms, so that the frequency shift can be calibrated with a known element, such as Xe.

C- Mass resolution

The standard deviation δf_0 is a function of the averaging time τ

$$\delta f_0 = \left[\frac{1}{N-1} \cdot \sum_{i=1}^N (\langle f_i^\tau \rangle - \langle f_0 \rangle)^2 \right]^{1/2} \quad (\text{S4})$$

with $\langle f_i^\tau \rangle$ the resonance frequency averaged over the time interval i with duration τ and $\langle f_0 \rangle$ the resonance frequency averaged over the whole measurement.

Another way to characterize the stability of a resonator is to use the Allan-like

deviation [4] $\sigma_A^2 = \frac{1}{N-1} \cdot \sum_{i=2}^N (\langle f_i^\tau \rangle - \langle f_{i-1}^\tau \rangle)^2 / \langle f_0 \rangle^2$

(S5)

We plot in Fig. S3 the Allan-like deviation (eq. S5) with the same data as in Fig. 2.

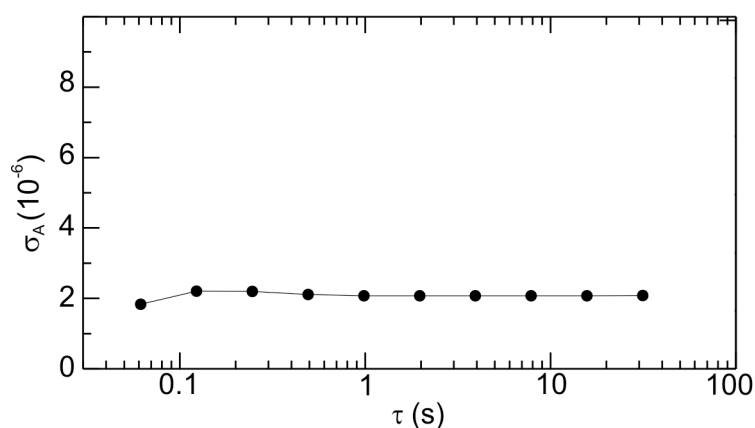


Fig. S3 Allan-like deviation of the resonance frequency as a function of the averaging time.

Figure S4 shows the measured time trace of I_{mix} from which we generate Fig. 2 and Fig. S3. The resonance frequency is so stable that the driving frequency in the computer-controlled feedback loop remains constant over the whole trace. The standard deviation of I_{mix} is 24.63 pA; the time between two measurement points is 62 ms. Using the measured current-frequency conversion (0.29 kHz/pA), we obtain that the standard deviation of f_{ref} is 7.144 kHz for $\tau = 62$ ms.

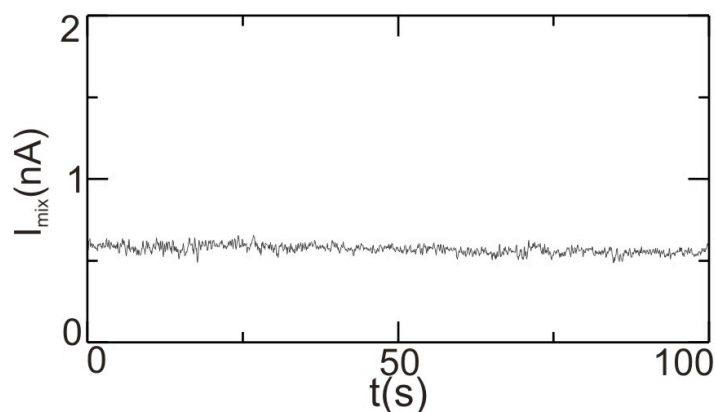


Fig. S4 Time trace of the mixing current corresponding to the measurements in Fig. 2.

The measured fluctuations could be accounted for by some diffusing molecules that remain on the nanotube surface or to the electrical noise of the nanotube. More work is needed to find the origin of the f_0 fluctuations. A possible way to further improve the mass resolution is to lower the temperature, which should reduce both the diffusion and the electrical noise.

Figure S5 shows the frequency stability of the resonator obtained in another measurement. The mass resolution is comparable to the one in Fig. 2, although its dependence on the averaging time is different.

We apply a relatively large excitation ($V^{FM} = 4$ mV), because the corresponding noise in the mixing current (24.6 pA in Fig. S4) is then larger than the noise in current of our measurement setup (typically 1-5 pA with 30 ms integration time). The disadvantage of this large excitation is that the resonance broadens and therefore lowers the slope that converts current to frequency. However, we experience that larger excitation overall enables better mass resolution.

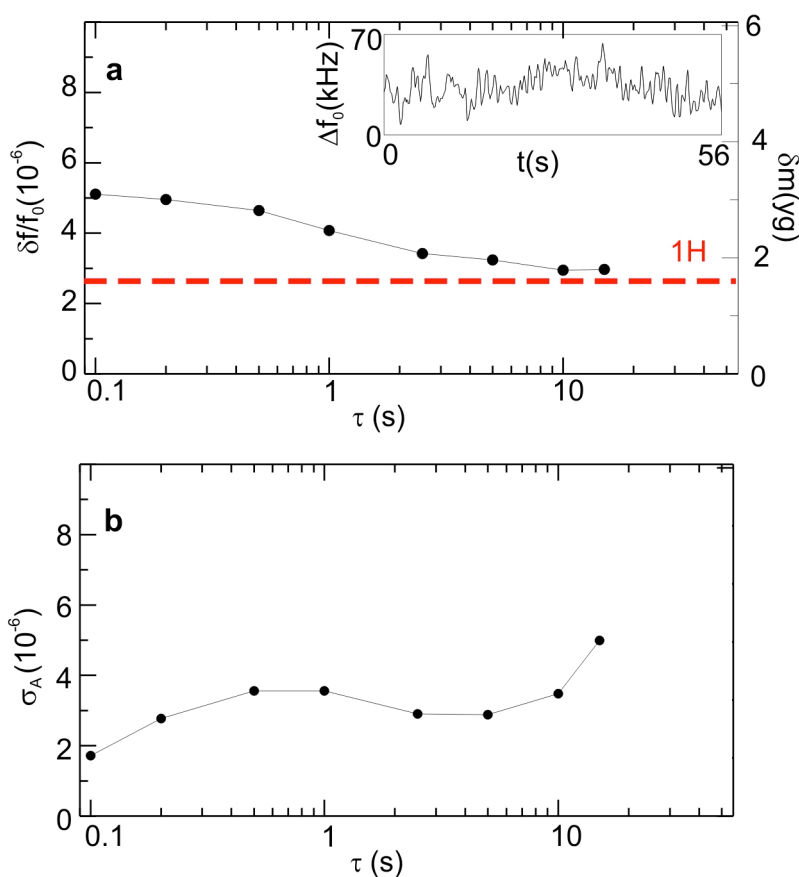


Fig. S5 Mass resolution. **a**, Standard deviation of the resonance frequency and the corresponding mass resolution as a function of the averaging time at 5.8 K. The inset shows the resonance frequency as a function of time. **b**, Allan-like deviation of the resonance frequency as a function of the averaging time.

D- Fluctuations in the resonance frequency

Figure 1e in the paper shows that the fluctuations of the resonance frequency f_0 are sizeable prior to the current annealing step. The resonance frequency fluctuates between multiple levels.

These multiple-levels fluctuations in Fig. 1e are not related to the noise in the electrical conductance of the nanotube, since they are also observed when continuously measuring the response I_{mix} versus f (Fig. S6).

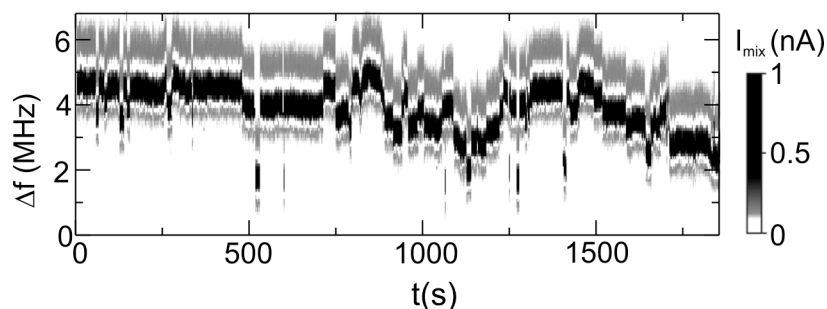


Fig. S6 Mixing current as a function of driving frequency and time. The resonance frequency follows the black trace. The time duration of one frequency sweep is 2.8 s. The amplitude of the applied FM voltage is 3 mV.

The multiple-level fluctuations in Fig. 1e are not due to electrostatic fluctuators. Electrostatic fluctuators have the same effect as shifting V_g and could thus change the resonance frequency (by changing the tension in the nanotube). An upper limit of the frequency shifts due to electrostatic fluctuators can be quantified from the fluctuations of the conductance. The maximum deviation of the conductance is 0.2 μS . Using a transconductance of 0.1 mS/V (which is the largest measured value when sweeping V_g between -10 and 10 V) we obtain a shift of V_g due to electrostatic fluctuators of at most 2 mV. The maximum shift of the resonance frequency is 14 kHz using the 7 MHz/V slope of the V_g dependence of f_0 (Fig. 1d). This is much lower than the multiple-levels fluctuations observed in Fig. S6 and Fig. 1e. This indicates that these multiple-levels fluctuations are not due to electrostatic fluctuators.

The multiple-level fluctuations are not due to adsorption and desorption of rest gas molecules in the ultra-high vacuum chamber either (we detect traces of H_2O , CO , and CO_2 using a commercial mass spectrometer). Indeed, these molecules remain in the chamber after the current annealing step, but the multiple-levels fluctuations are no more present (Fig. 1e).

The shifts in f_0 between these multiple levels occur frequently after cooling the resonator from high temperature (above 150 K) down to liquid helium temperature. As the resonator is cooled down, rest gas molecules get adsorbed onto the

nanotube. This suggests that the origin of the multiple-level fluctuations is related to a few molecules diffusing on the nanotube surface between various trapping sites. These molecules may move either individually or collectively. The current annealing step removes these molecules from the nanotube surface.

A lower bound for the diffusion constant of these moving molecules can be inferred from the multiple-level fluctuations measured at 6 K in Fig. 1e. We obtain

$D = L^2 / \tau > 10^{-14} \text{ m}^2\text{s}^{-1}$ by taking $L = 0.1 \text{ } \mu\text{m}$ and using $\tau < 1 \text{ s}$; the upper bound for the diffusion time corresponds to the typical time for the computer-controlled feedback loop to retrieve the resonance after a large frequency jump (the jumps between the multiple levels are so fast that the computer-controlled feedback loop cannot track the variation of f_0).

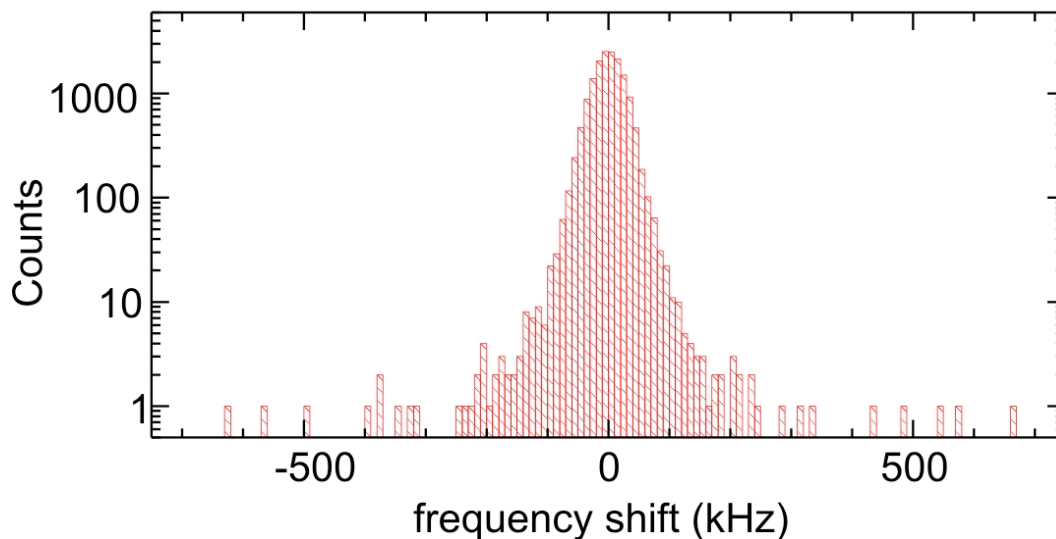


Fig. S7 Histogram of the frequency difference between adjacent measurement points in Fig. 1e before current annealing.

Figure S7 shows the histogram of the frequency difference between adjacent measurement points in Fig. 1e (before current annealing). The histogram shows a large symmetric peak flanked by a few events occurring at large negative and positive frequency shifts (with counts up to 10 in Fig. S7). These few high-frequency events correspond to the jumps observed in the time trace in Fig. 1e. These events are distributed quite homogeneously in frequency so it is difficult to correlate them to the mass of the molecules that are present in the chamber, that is, H_2 , H_2O , CO , and CO_2 . The central peak is quite broad: the standard deviation of the frequency shifts is 35 kHz, which is larger than that measured after current annealing (5.1 kHz).

In order to be able to correlate the high-frequency events to the mass of molecules, we need more points for these events. For this, we will acquire longer time traces. We will also increase the temperature in an attempt to enhance the rate of these events.

When dosing xenon or naphthalene atoms, our measurements (e.g. in Fig. 3a) do not allow us to identify prominent features in the histogram of the frequency shifts, which could be used to shed light on the desorption-diffusion process. An interesting route will be to carry out noise measurements, similar to those of Yang and coworkers [5], in order to quantify the diffusion of dosed atoms and molecules.

E- Monitoring adsorption of xenon atoms and naphthalene molecules

Figure S8 shows the resonance frequency as a function of time while dosing naphthalene molecules. The resonance frequency shows a tendency to decrease, indicating that naphthalene molecules are being adsorbed on the nanotube. Abrupt upward shifts in f_0 as high as ~ 2 MHz are also detected (red arrows). This measurement shows the same trend as in Fig. 3a where Xe atoms are dosed.

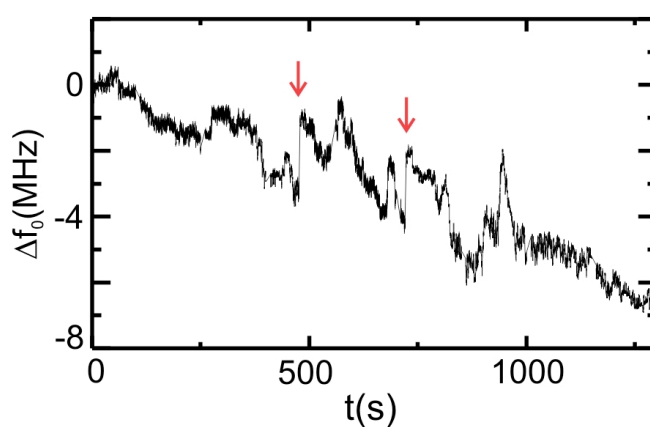


Fig. S8 Adsorption of naphthalene molecules. Resonance frequency is shown as a function of time at 4.5 K when naphthalene molecules are dosed. The resonance frequency is measured using the computer-controlled feedback loop. Red arrows indicate abrupt upward shifts (the variation of f_0 is so sudden that the feedback loop cannot record any data point during the upward shift). The dosing rate is not held constant; it varies between 0.03 and 0.3 1/s (the rate is estimated from the measured pressure).

Figure S9 shows the different resonance lineshapes recorded by the computer-controlled feedback loop during the measurement in Fig. S8. In the last 4 resonance traces, the lineshapes are noisy and the resonance height is lower than at the

beginning. If the lineshapes were to deteriorate further, we would not rely on the output of the feedback loop.

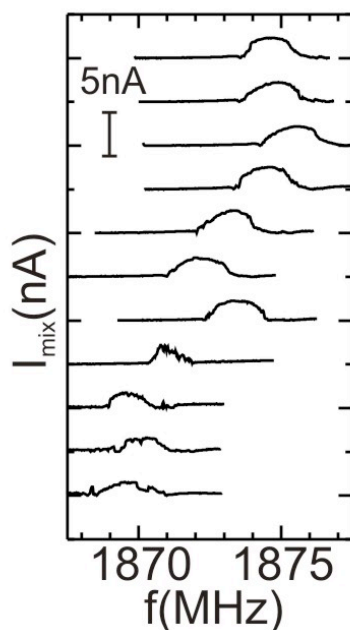


Fig. S9 Control of the resonance lineshape. During the measurement shown in Fig. S8, the feedback is interrupted every 150 s for a control of the lineshape of the resonance.

Figure S10a shows a series of resonance frequency downward shifts obtained by dosing Xe atoms onto the nanotube (f_0 is indicated by a red dot). These resonance frequency downward shifts are consistent with the adsorption of individual (or a few) Xe atoms. We note that the lineshape of the resonances is rather noisy and changes from one measurement to the next, probably because of the diffusion process discussed in the paper. Indeed, the lineshape of the resonances before dosing Xe atoms are much less noisy; we obtain that the standard deviation of the resonance frequency is 96 kHz (f_0 being obtained by fitting the resonances) which is much lower than the uncertainty of about 0.5 MHz in the determination of f_0 in Fig. S10. The shaded area in Fig. S10b shows upward shifts of the resonance frequency. These upward shifts might be related to individual (or packets of) Xe atoms that either desorb into the vacuum or diffuse along the nanotube towards the clamping regions.

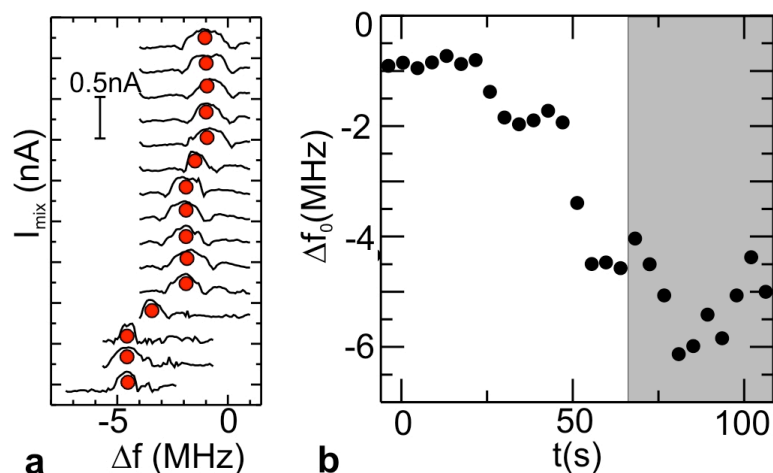


Fig. S10 Adsorption of Xe atoms. Resonance frequency is shown as a function of time at 6 K when Xe atoms are being dosed onto the nanotube. The resonance frequency is obtained by continuously measuring I_{mix} as a function of f . Xe atoms arrive directly from the microdoser onto the nanotube so the dosing rate cannot be determined. **a**, Series of mixing current responses versus drive frequency, which are measured as a function of time. **b**, Resonance frequency as a function of time. Dots in the white area correspond to the resonance frequencies measured in a.

Our adsorption measurements in Fig. 4 show that the Xe-nanotube binding energy is about 130 meV. In this respect, it is rather surprising that an impinging Xe atom that originates from a 300 K reservoir can trigger the desorption or the diffusion of Xe atoms. An explanation might be that since impinging Xe atoms arrive with different energies (distributed according to the Boltzmann distribution), the desorption-diffusion process is only triggered by the Xe atoms with energy larger than 130 meV. Moreover, although the energy barrier against diffusion of Xe on a nanotube is not known, it should be a fraction of the binding energy and could be well below 25 meV. In addition, the desorption might occur at a defect or a contaminated site of the nanotube where the binding energy is also lower. The origin of the desorption-diffusion trigger is unclear and calls for future work.

As for naphthalene, the physics of adsorption and molecule-molecule interaction is even more complex, since it is a large molecule that is highly anisotropic and has multiple internal degrees of freedom. The naphthalene-graphite binding energy is about 850 meV [6]. The number of degrees of freedom is $3N = 54$, since the number of atoms is $N=18$. The average energy per molecule is thus significantly higher than 25 meV and somewhat lower than $3NkT/2 = 700$ meV using $T = 300$ K.

F- Adsorption measurements of Xe atoms

Figure S11a shows the number of Xe atoms on the nanotube as a function of $1/T$ for two different cooling rates. The two measurements are very similar. The slope yields $E_b = 131$ meV. Figure S11b shows the measurement for another nanotube resonator and the slope yields $E_b = 110$ meV.

This behavior can be accounted for by the balance of Xe atoms impinging on and departing from the nanotube. We assume that the rate of atoms impinging on the nanotube $(dN_{Xe}/dt)_{ON}$ is a constant given by the dosing rate and the nanotube surface, whereas the rate of atoms departing from the nanotube is

$$(dN_{Xe}/dt)_{OFF} = (N_{Xe})^n \gamma \exp(-E_b / k_B T) \quad (S6)$$

where n is the order of desorption, γ the attempt frequency and E_b the binding energy [7,8]. We set $n = 1$ since the coverage is low and that Xe atoms are expected to interact essentially with the nanotube surface and only weakly with other Xe atoms. Measurements are carried out at a low cooling rate so that the system can equilibrate at each measurement temperature and we expect that $(dN_{Xe}/dt)_{ON} = (dN_{Xe}/dt)_{OFF}$. As a result, we obtain

$$N_{Xe} \propto \exp(E_b / k_B T) \quad (S7)$$

We note that the good agreement between the model and the measurements in Fig. S11 further supports our assumption that $n = 1$.

We employ the term ‘adsorption’ in this work for the process where an atom impinges the nanotube *and* remains on its surface. When measurements are described by Eq. S7, adsorption is a thermally activated process.

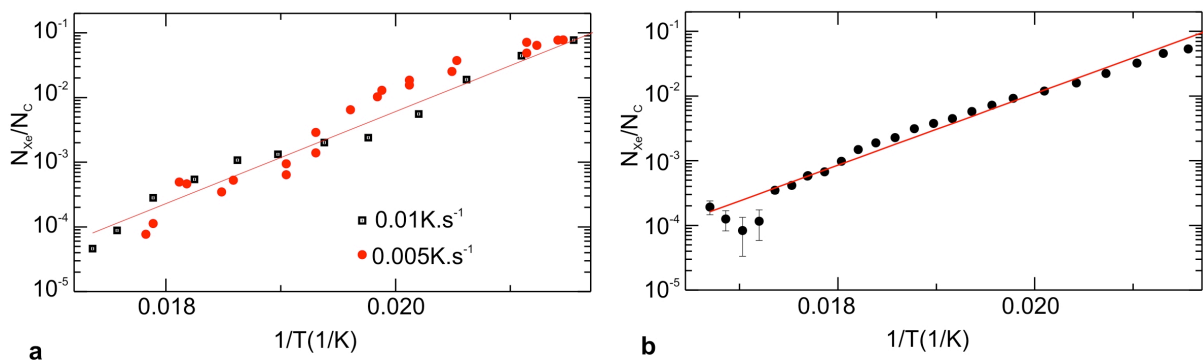


Fig. S11 Adsorption of Xe atoms. a, Number of Xe atoms per C atom as a function of $1/T$ at two different cooling rates. Xe atoms are being dosed onto the nanotube at

a rate of ~22 atoms/s. The nanotube is the same as the one in Fig. 4a. **b**, Number of Xe atoms per C atom as a function of $1/T$ for another nanotube resonator. The dosing rate is ~22 atoms/s. The diameter of the nanotube is $d = 2.3$ nm and the length of the suspended nanotube section is $L_{tube} = 1200$ nm.

G- Calculation of the xenon-nanotube binding energy

The van der Waals interaction between the Xe atom and the nanotube is described by means of a pairwise Lennard-Jones potential where the potential energy is given by:

$$E = \sum_{C_i} 4\epsilon \left[\left(\frac{\sigma}{r_{Xe-C_i}} \right)^{12} - \left(\frac{\sigma}{r_{Xe-C_i}} \right)^6 \right] \quad (S8)$$

where the sum runs over all the carbon atoms and r_{Xe-C_i} is the Xe-C distance; we take the values $\sigma = 3.332$ Å and $\epsilon = 11.025833$ meV [9], a parameterization of the Xe-C interaction fitted to reproduce the experimental Xe-C distance and binding energy in graphite [10]. Effects of the corrugation, not taken into account here, can be emphasized by including anisotropic corrections to the potential [11].

We determine the most stable adsorption site of Xe on graphene. For this, we select high-symmetry points on the graphene lattice, which are candidates to yield local minima in the energy landscape: on top of a C atom (T), above a hexagon center (H) and above the center of a C-C bond (B). We use a 9×9 supercell of the 2-atom primitive cell. We find that Xe favors adsorption at the center of a hexagonal C ring, in agreement with published results for graphite [9].

Next, we focus on the adsorption potential of the H site, the preferential binding configuration of Xe. We sample the adsorption potential by approaching the Xe atom to the nanotube surface from 10 to 2 Å, by steps of 0.035 Å. The procedure is repeated for diameters ranging from 0.6 to 4.1 nm. We use a $1 \times 1 \times 10$ supercell of the primitive cell of the armchair nanotube. The interaction energy as a function of the xenon-nanotube separation is shown in Fig. 4b. Figure 4c shows that as the diameter of the nanotube increases, the binding energy increases too. The reason for this dependence on the diameter of the nanotube is merely geometric. The nanotube curvature modifies the distance between the Xe atom and most of the C atoms (upper inset of Fig. 4a). The van der Waals interaction, here modeled by the Lennard-Jones potential, has a very long range and even C atoms relatively far from the Xe atom contribute in a non-negligible way to the interaction energy.

References

- [1] Gouttenoire, V., Barois, T., Perisanu, S., Leclercq, J.-L., Purcell, S. T., Vincent, P., & Ayari, A. Digital and FM Demodulation of a Doubly Clamped Single-Walled Carbon-Nanotube Oscillator: Towards a Nanotube Cell Phone. *Small* **6**, 1060-1065 (2010).
- [2] Eichler, A., Moser, J., Chaste, J., Zdrojek, M., Wilson-Rae, I. & Bachtold, A. Nonlinear damping in mechanical resonators made from carbon nanotubes and graphene. *Nature Nanotech.* **6**, 339-342 (2011).
- [3] Naik, A. K., Hanay, M. S., Hiebert, W. K. , Feng, X. L. & Roukes, M. L. Towards single-molecule nanomechanical mass spectrometry. *Nature Nanotechnology* **4**, 445-450 (2009).
- [4] Feng, X. L., White, C.J., Hajimiri, A., & Roukes, M.L. A self-sustaining ultrahigh-frequency nanoelectromechanical oscillator. *Nature Nanotech.* **3**, 342-346 (2008).
- [5] Yang, Y.T., Callegari, C., Feng, X. L. & Roukes, M. L. Surface adsorbate fluctuations and noise in nanoelectromechanical systems. *Nano Lett.* **11**, 1753-1759 (2011).
- [6] Zacharia, R., Ulbricht, H. & Hertel, T. Interlayer cohesive energy of graphite from thermal desorption of polyaromatic hydrocarbons. *Phys. Rev. B* **69**, 155406 (2004).
- [7] Polanyi, M. & Wigner, E. Concerning the interference of natural oscillation as a reason for energy variations and chemical transformation. *Zeitschrift fur Physikalische Chemie* **139**, 439 (1928).
- [8] Miller, J. B., Siddiqui, H.R., Gates, S.M., Russell, J.N. & Yates, J.T. Extraction of kinetic parameters in temperature programmed desorption: A comparison of methods. *J. Chem. Phys* **87**, 6725-6732 (1987).
- [9] Simonyan, V.V., Johnson, J. K., Kuznetsova, A. & Yates, J. T. Molecular simulation of xenon adsorption on single-walled carbon nanotubes. *J. Chem. Phys.* **114**, 4180-4185 (2001).
- [10] Vidali, G., Ihm, G., Kim, H.-Y. & Cole, M. W., Potentials of physical adsorption. *Surf. Sci. Rep.* **12**, 135-181 (1991).
- [11] Carlos, W. E. & Cole, M. W. Interaction between a He Atom and a Graphite Surface. *Surf. Sci.* **91**, 339-357 (1980).